Open Access

OBM Transplantation

LIDSEN Publishing Inc.

Original Research

Design and Simulation of Computational Models of Hybrid Scaffolds Representative of Subchondral Bone and Hyaline Cartilage

Jessica Palacios [1], Odin Ramírez-Fernández [2, 3], Esmeralda Zuñiga-Aguilar [1, *]

1. Instituto de Ingeniería y Tecnología de la Universidad Autónoma de Ciudad Juárez, Juárez, Chih, México; E-Mails: ess.parm@gmail.com; esmeralda.zuniga@uacj.mx
2. Universidad Politécnica de Cuautitlán Izcalli, Cuautitlán Izcalli, Méx, México; E-Mail: odinramirezfernandez@gmail.com
3. Universidad Tecnologica de Mexico-UNITEC Mexico-Campus en Linea, Av. Marina Nacional No. 162, Col. Anáhuac, Ciudad de México CP.11320, México

* **Correspondence:** Esmeralda Zuñiga-Aguilar; E-Mail: esmeralda.zuniga@uacj.mx

Academic Editor: Eric M. Bluman

Special Issue: Bone Grafting in Trauma and Elective Orthopaedics

OBM Transplantation
2025, volume 9, issue 1
doi:10.21926/obm.transplant.2501240

Received: August 22, 2024
Accepted: March 03, 2025
Published: March 07, 2025

Abstract

Tissue engineering offers alternatives when it comes to health problems such as trauma or pathologies. One of them is the scaffolds, which provide a favorable architecture, mechanics, and biocompatibility for the fixation of cells. Therefore, the following research aims to design and simulate scaffolds with mixed geometric structures to create a hybrid architecture for osseointegration while maintaining structural properties similar to subchondral bone and hyaline cartilage. Three scaffolds were designed for this purpose, with mixed geometric shapes inside: squares for trabecular bone, hexagons for subchondral bone, and octagons for hyaline cartilage, each with a specific pore size according to the architecture and biomechanics of each tissue. SolidWorks computer-aided design software to design unit cells for each particular tissue, followed by the Ansys Workbench integrated simulation platform to simulate the loads produced by an average-weight adult typically used in walking. We used two specific materials (Hydroxyapatite and Vitreous Humor with sodium alginate) that are

part of the hydrogel for its possible future use in the 3D printing of these models. Different results were obtained from the models presented. Still, the truncated pore and gradual pore models were found to be close to the actual parameters for subchondral bone and cartilage, respectively, giving Young's modulus of 1049.5124 MPa in the subchondral bone region and 9.4086 MPa in the cartilage region. Therefore, we concluded that combining the architectures of these two models into one offered the possibility of creating a scaffold capable of mimicking the osteochondral complex.

Keywords
Scaffolds; hyaline cartilage; subchondral bone; osteochondral complex; chondral injuries; design; simulation; biomechanics; young's modulus

1. Introduction

For the clinical application of tissue engineering, the use of scaffolds facilitates the creation of tissues. Scaffolds are temporary structures or supports that enable cells to grow and form tissue [1]. When designing and manufacturing them, it is crucial to consider the properties of the tissue to be regenerated, the characteristics of the scaffold to be developed, the biocompatibility of the materials, and their mechanical, biological, and physicochemical properties [1]. For this reason, composite materials or structures (hybrids) should be capable of mimicking a tissue in cases of trauma or pathologies that require regeneration. Chondral injuries occur when excessive loads or trauma damage the articular cartilage. These injuries can be categorized into different grades based on the Outerbridge scale, with Grade IV being the most severe; in this type, articular cartilage wear is characterized by damage and exposure to the subchondral bone [2]. Procedures for repairing chondral wounds range from the treatment of microfractures to replacement with a partial or total prosthesis. The non-prosthetic techniques can be classified into three categories: reparative methods, which help form fibrocartilage and provide access to the vessels and cells that generate chondrocytes; reconstructive methods, which focus on filling the lesion with grafts; and regenerative methods, which promote the development of hyaline cartilage through tissue engineering [3].

Scaffolds permit the formation of tissues with significant potential for application. However, to achieve this, it is essential to meet specific requirements, including preserving tissue structure to enable cellular processes such as growth, differentiation, and distribution, as well as providing chemical and biological substances for this purpose. For these structures, whether synthetic or natural, to possess the capacity to form tissues, they must exhibit characteristics that emulate the shape, structure, and function of the tissue in such a way that it can be integrated into the surrounding environment. The complexity lies in the characteristics and properties, as numerous factors, including porosity, pore size, mechanical properties, density, cell type, age, and state of health, among others [4]. An emerging strategy is using lattice structures to construct scaffolds [5]. According to Tang [6], lattice structures are more flexible and customizable to achieve a desired physical property. In addition, 3D printing allows for generating lattice structures with properties like bone and potentially improves mechanical efficiency [7, 8]. Using suitable materials and

structures significantly influences scaffold design; models with rectangular, cubic, and octahedral pores are more appropriate for bone mimicry, oxygen transport, and fluid permeability [9, 10]. The design of osteochondral scaffolds can be used to create biphasic or triphasic structures, varying the physical properties in different layers depending on the depth, which provides an approach to cartilage and bone development [11-13].

Therefore, the primary motivation of this work is to present the results of simulation studies of cell growth scaffolds, according to the designs made with mixed geometric lattice-type structures, to provide scaffolds with a hybrid architecture that can promote tissue osseointegration and provide mechanical properties similar to those of subchondral bone and hyaline cartilage.

2. Materials and Methods

Three different models of scaffolds with mixed figures inside, with a phase for cartilage, another for subchondral bone, and another for trabecular bone. Each one had different geometry and pore size specifications that varied according to the design of each model.

All scaffolds were designed with support dimensions of 6 × 10 mm in height, divided into three sections: 5 mm for the cartilage area, 3 mm for the subchondral bone area, and 2 mm for the trabecular bone area, as illustrated in Figure 1.

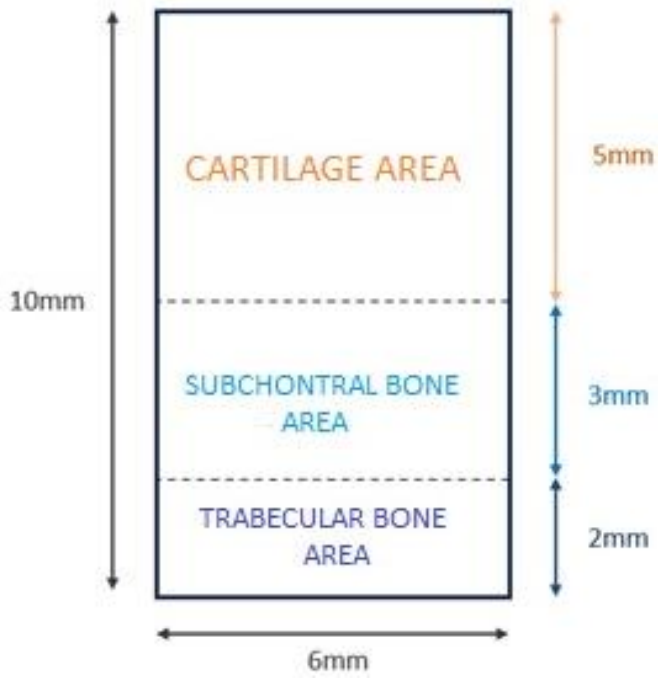

Figure 1 Model base scheme.

Each cell was reproduced longitudinally and transversely on the surfaces of the scaffolding to create the basic scheme of Figure 1, ensuring similarity in dimensions; each pattern was designated based on the unique characteristics of each one. The defined scaffolding was called this because each zone was placed with a delimitation so that the pores destined for each tissue were defined and separated. For the truncated pore scaffolding, three unit cells were designed and made from a hollow hexahedron to create a thickness between pores thinner than the defined scaffolding, each with its respective dimensions and assigned pore geometries. Finally, with the gradual scaffold, a

distinction emerged between two different unit cells, resulting in a transition zone where the geometries for cartilage and bone intermingled within the central space designated for subchondral bone. The pore sizes and geometries implemented were as follows: cartilage area: oval and octagonal pores with a diameter of 250 µm; subchondral bone area: hexagonal pores with a diameter of 200 µm; trabecular bone area: square pores with a diameter of 500 µm.

2.1 Biomaterials

For the simulation, the biomaterials used were hydroxyapatite for the bone area and vitreous humor for the cartilage area; rheology obtained values experimentally. Table 1 shows the properties used for the finite element analysis, admitting an isotropic behavior.

Table 1 Parameters used for the simulation [10, 14].

Materials	Young's modulus (E)	Poisson's ratio
Hydroxyapatite	2000 MPa	0.3
Vitreous humor and sodium alginate	19.6 MPa	0.4

2.2 Simulation

The loads faced by a healthy knee in a two-legged stance (2L) and one-legged stance (1L) were considered for the simulation, movements typically used in walking. For 2L, authors found that 46% of the body weight acts in this stance in the axis direction, and, on the other hand, the change of position from 2L to 1L causes an increase in forces of approximately 2.5 times [8, 12, 15]. Given the above, considering, it accounts for the average weight of 70 kg (Table 2).

Table 2 Loads used in the simulation.

Position	Weight	Strength	Load
2 Legs (2L)	70 kg	46%	315.88 N
1 Leg (1L)	70 kg	115%	789.70 N

3. Results

3.1 Unit Cells

As mentioned in the methodology, three distinct unit cells were designed for the defined and truncated pore models. In contrast, two cells for the truncated pore model were spread throughout the scaffold. Figure 2 displays the results of these cells, and the models shown below were developed.

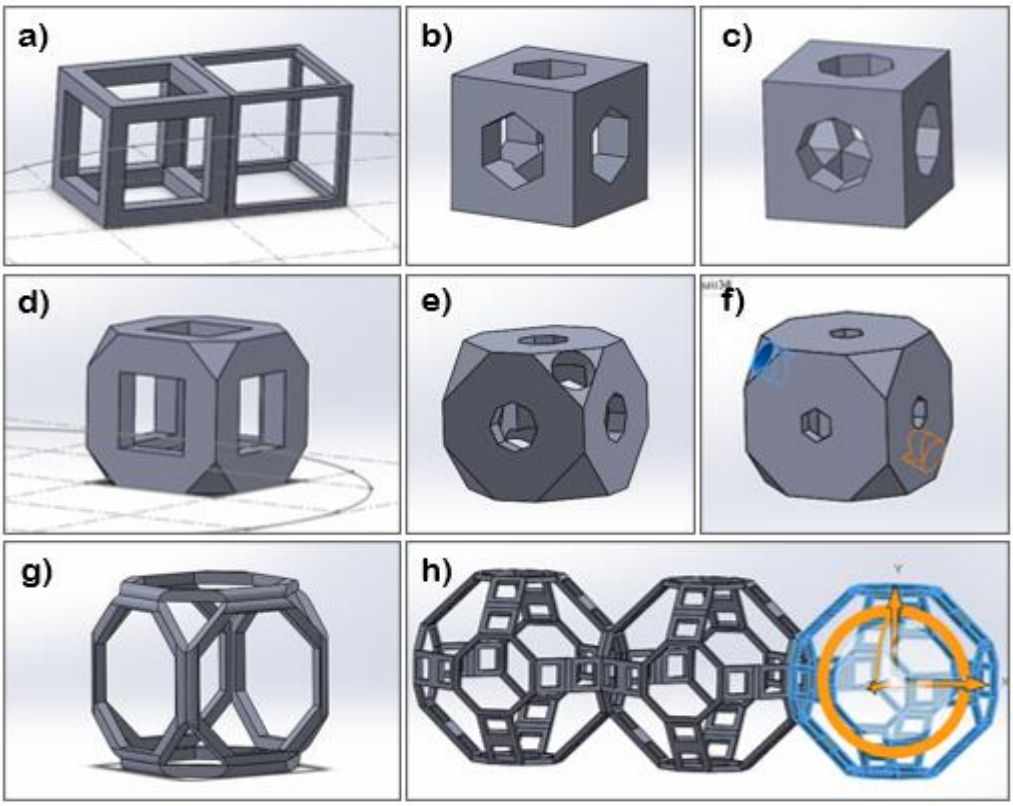

Figure 2 Unit cells used in the defined model: a) trabecular bone, b) subchondral bone, and c) cartilage. Unit cells used in the truncated pore model: d) trabecular bone, e) subchondral bone, and f) cartilage. Unit cells used in the gradual model: g) bone, and h) cartilage.

In the third model, which corresponds to the gradual scaffolding, the purpose was to design a lower-density structure using two unit cells (see Figure 2) instead of three, as in the previous designs. The two cells were distributed gradually at approximately 3 mm, as shown in Figure 3.

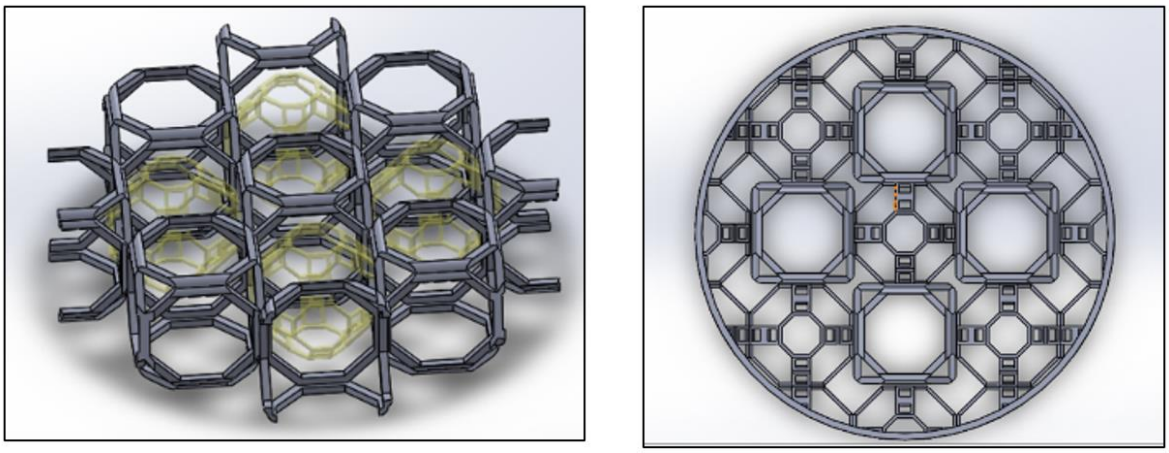

Figure 3 Graded areas of the scaffold with unit cells between mixed, predominantly bone cells on one (right side) and predominantly cartilage cells on the other (left side).

This gradual structure between the two distinct areas of the scaffold has been identified in other studies, where it is referred to as an interface zone between cartilage and bone. This interface zone has been observed to promote the subchondral bone as a mediator in cartilage formation, leading to repair. This finding is supported by evidence from previous studies [16, 17]. The laminate thickness of the bone unit cell was 100 µm, resulting in a bonded thickness of 200 µm. The laminate thickness of the cartilage unit cell was 50 µm, resulting in a bonded thickness of 100 µm. These values align with those observed in a recent investigation employing additive manufacturing methods [18].

3.2 Models and Meshing

The base dimensions used for the design of the scaffolds were 10 mm in height and 6 mm in base, taken as a reference since in transplant approaches for chondral defects, the height is usually 8 to 10 mm for defects more significant than 4 cm^2 [19]. Even in a study for osteochondral tissue regeneration with biphasic scaffolds, these exact dimensions were used [16]. Regarding the area designated for each tissue in the introduction section, the approximate thicknesses of each tissue of the osteochondral complex are mentioned thus: 5 mm for cartilage, 3 mm for subchondral bone, and the remaining 2 mm were intended for the osseointegrate part. The exact measurements mentioned were not applied to each section of the models since they varied depending on the design of the models.

The defined model resulted in a final height of 7.8 mm, 2.1 mm in the area, for trabecular bone replicated in its interior 207 unit cells distributed in three levels (69 cells per level). 2.8 mm in the area for subchondral bone inside 276 unit cells distributed in four levels (69 cells per level) with a delimitation of 0.05 mm between the previous areas. 3.5 mm in the area for cartilage replicated inside 345 unit cells distributed in five levels (69 cells per level) with a delimitation of 0.05 mm between the anterior regions. Figure 4A shows the result of the model.

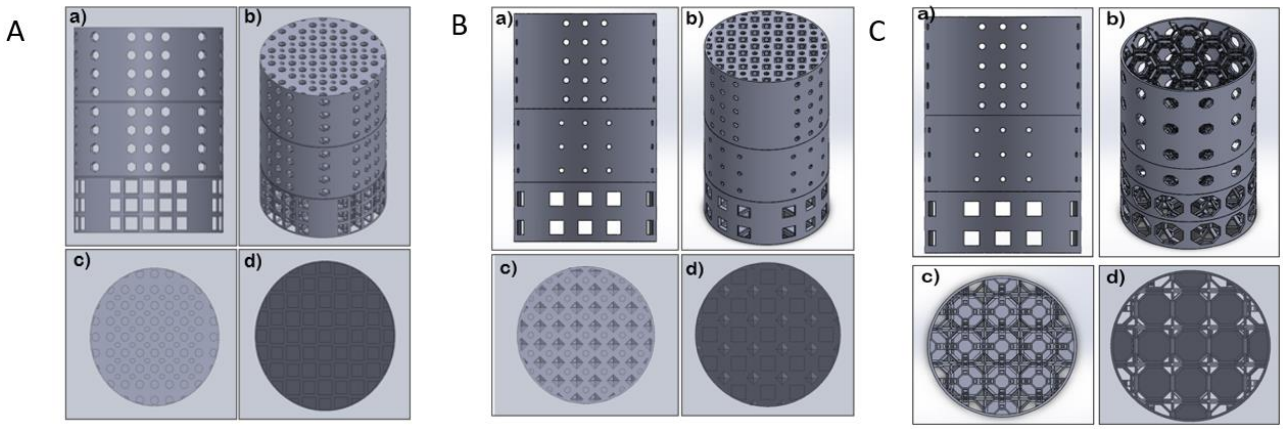

Figure 4 A. Views of the defined model: a) frontal, b) isometric, c) top, d) base. B. Views of the truncated pore model: a) frontal, b) isometric, c) top, d) base. C. Views of the gradual model: a) frontal, b) isometric, c) top, d) base.

The truncated pores model resulted in a final height of 9.6 mm; 2.5 mm in the area for trabecular bone replicated inside 42 unit cells distributed in 2 levels (21 cells per level). In the region, 3.1 mm for subchondral bone inside 81 unit cells distributed in three levels (27 cells per level). 4 mm in the

area for cartilage replicated inside 225 unit cells distributed in five levels (45 cells per level). Figure 4B shows the result of the model.

The gradual model resulted in a final height of 9.34 mm: 1.61 mm in the area for bone replicated inside 20 unit cells distributed in a single level. 3.14 mm in the gradual area inside 42 unit cells distributed in three levels (21 cells per level). 4.59 mm in the area for cartilage replicated inside 63 unit cells distributed in three levels (21 cells per level), (see Figure 4).

A mesh with tetrahedral in its geometry represents an enjoyable alternative, as it accurately represents curved boundaries without deforming the base model. Furthermore, a study conducted to simulate deformations in the articular surfaces using finite elements indicates that this method yields favorable accuracy and computational cost results. The defined model yielded 630,827 nodes and 334,109 elements, while the truncated pore model resulted in 456,982 nodes and 242,780 elements. The gradual model yielded 886,222 nodes and 434,631 elements at a resolution of 4, resulting in a mesh of an appropriate size and time execution.

3.3 Compression Stress Tests

3.3.1 Defined Model

Compression tests began with a force of 315.88 N, corresponding to position 2L, in the defined model. The highest stress for this test was in the subchondral bone zone, with a maximum value of 184.5 MPa as shown in Figure 5A, while the remaining zones presented similar values ranging between 0.0408 MPa and 105.45 MPa. The zones for subchondral and trabecular bone resulted in having the same deformation with values between 5.87E-05 MPa and 1.3759 MPa, being the zone for cartilage the one that presented more, with a maximum value of 5.5033 MPa shown in Figure 5B. Suppose we observe the total displacement, shown in Figure 5C. In that case, it is noticeable that the only area that shows displacement is destined for cartilage, where compression is concentrated on the surface until it gradually decreases to zero before reaching other regions.

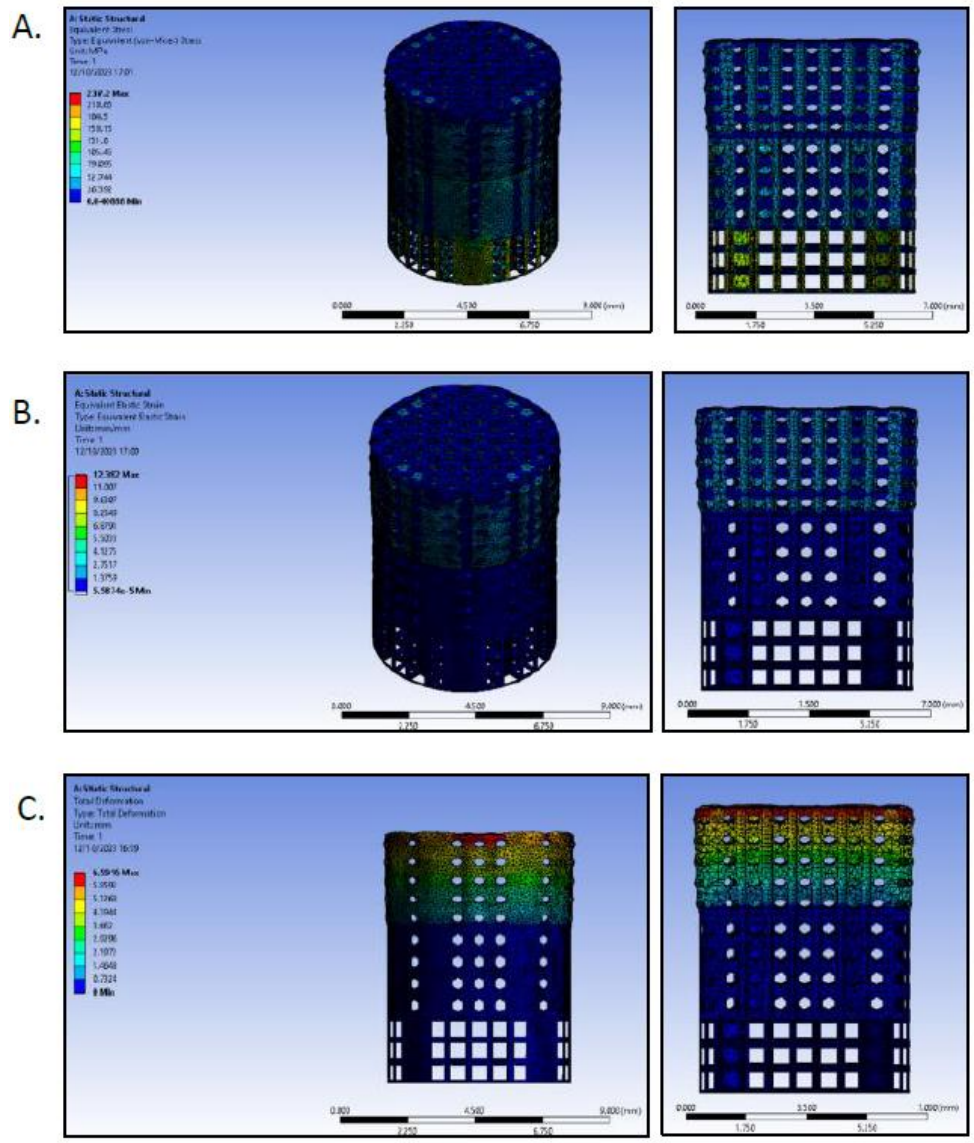

Figure 5 A. Stress distribution with an applied compressive force of 315.88 N for a defined model. B. Strain with an applied compressive force of 315.88 N for the defined model. C. Total displacement with an applied compressive force of 315.88 N for the defined model.

The simulation results for position 1L with an applied force of 789.70 N were very similar to those of position 2L; Figure 6 compares these values.

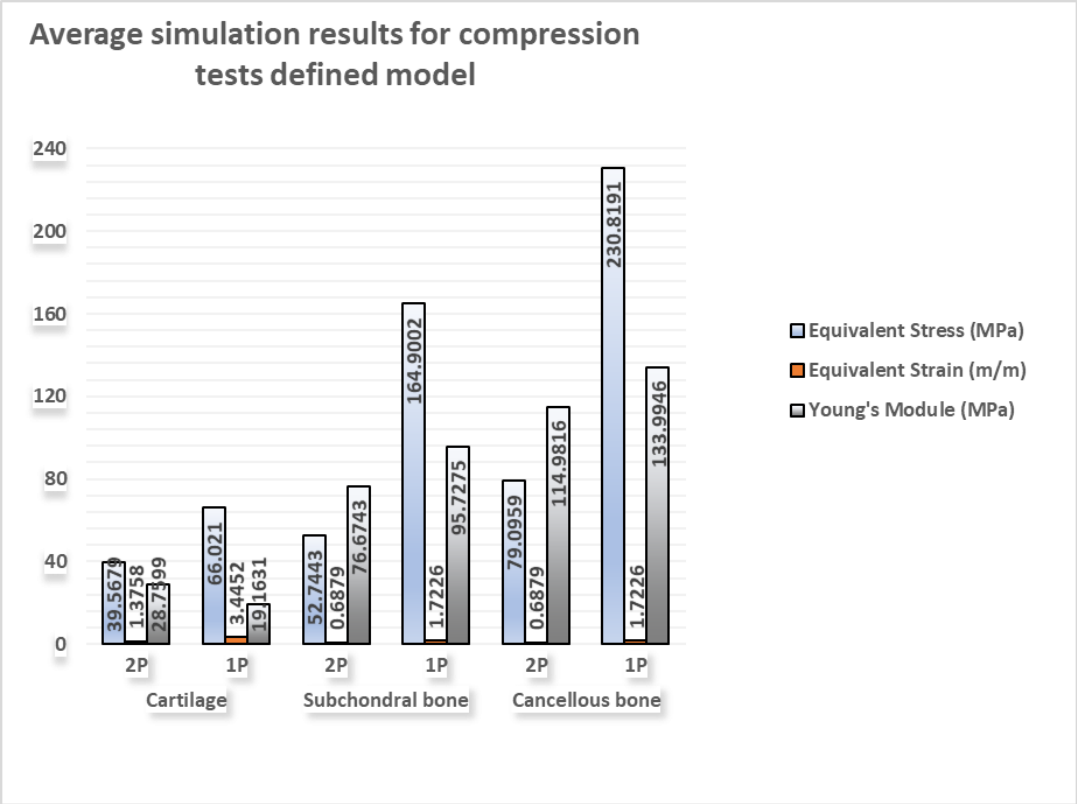

Figure 6 Compression tests in the defined model.

3.3.2 Truncated Pores

In the truncated pores model, we have an equal stress concentration for all areas and low; the whole model resulted in 936.48 MPa in the stress distribution, indicated with dark blue in Figure 7A as the lowest. In green and light blue colors, the most deformation was localized only in the zone for cartilage with 1.7846 to 5.3538 mm/mm, and just starting the zone for subchondral bone, the values decreased with almost zero, as shown in Figure 7B. The total displacement continued to show identical behavior to the previous tests, as shown in Figure 7C.

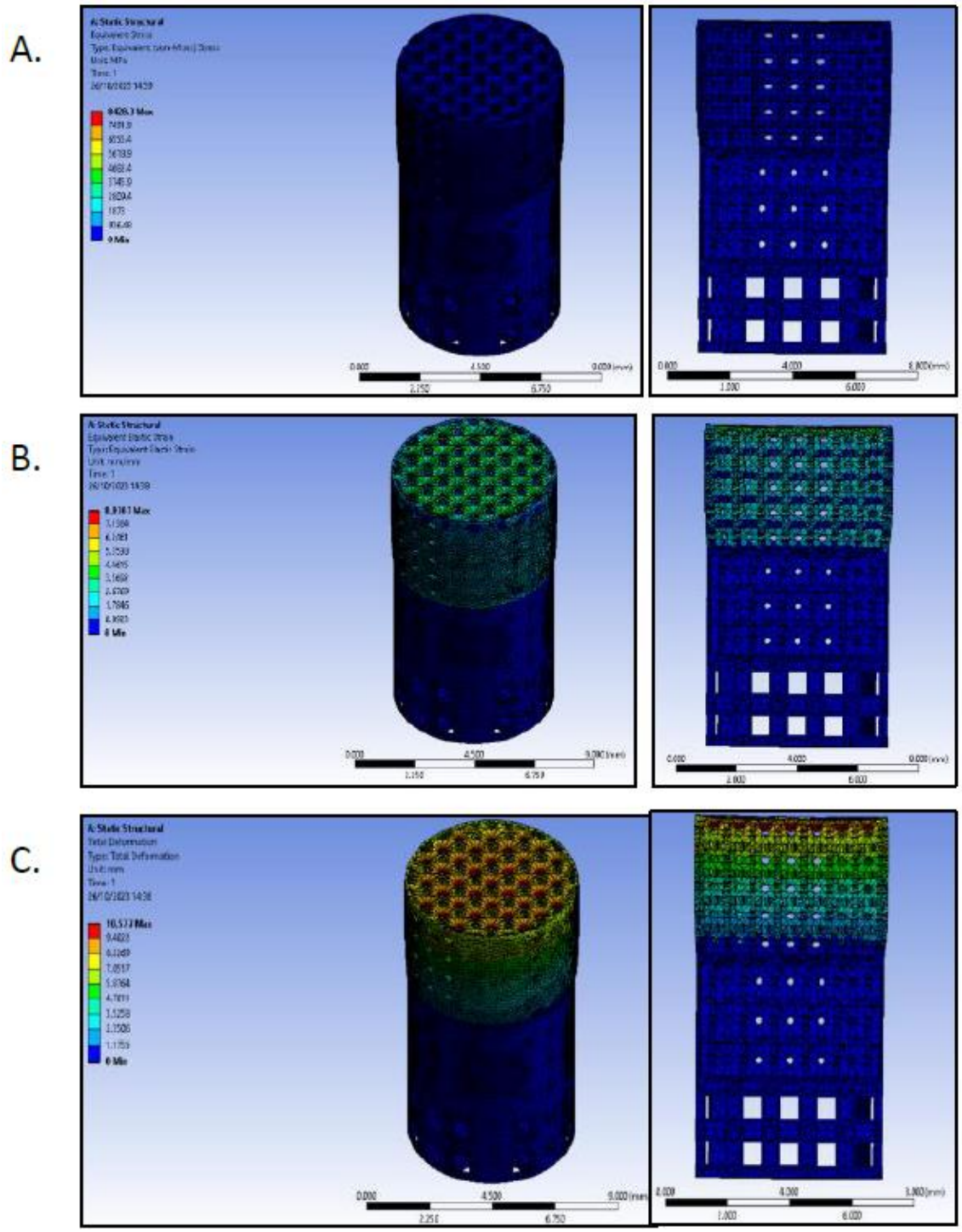

Figure 7 A. Stress distribution with an applied compressive force of 315.88 N for the truncated pore model; B. Strain with an applied compressive force of 315.88 N for the truncated pore model; C. Total displacement with an applied compressive force of 315.88 N for truncated pore model.

The simulation results for position 1L with an applied force of 789.70 N were very similar to those of position 2L, like in the case of the previous model. Figure 8 shows a comparison of these values.

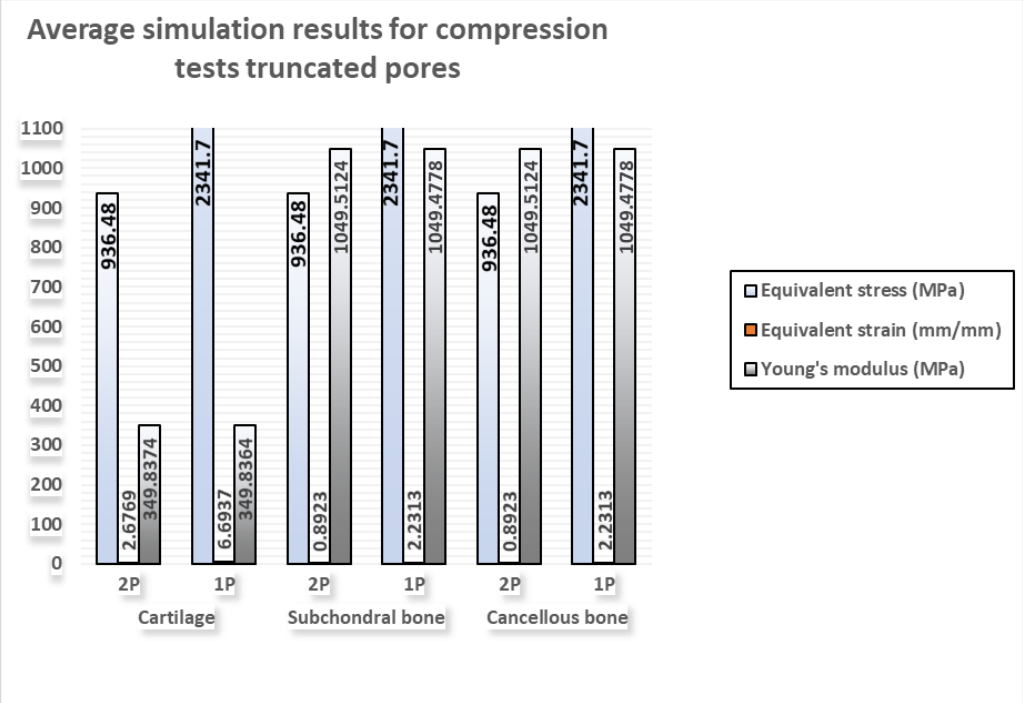

Figure 8 Average simulation results for truncated pores model compression tests.

3.3.3 Gradual Model

In the gradual model, at first glance, it seems that the stress distribution is the same for all areas; if we look more closely at Figure 9A, there are sections with light colors inside, specifically in cartilage and trabecular bone, where the values ranged between 782.86 and 0.0109 MPa. Figure 9B shows that the deformation in the area for cartilage varied between 83.208 MPa and 1.2295E-05 MPa. In contrast to 41.604 MPa and 1.2295E-05 MPa in the regions for bone. The displacement showed a behavior of more significant compression towards the center (see Figure 9C), without deforming the bone zone, except for a small section where the unit cells were for bone and cartilage (mostly cartilage).

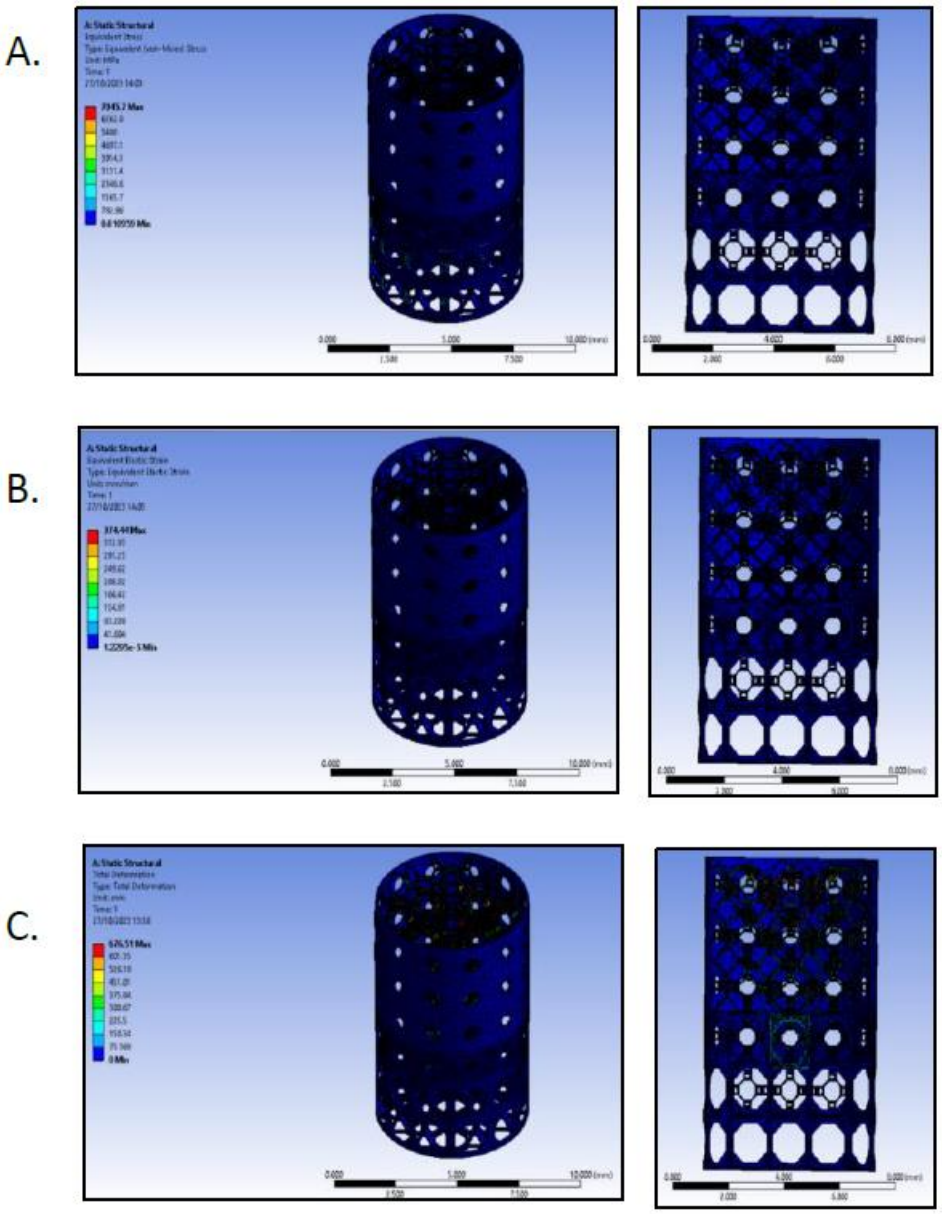

Figure 9 A. stress distribution with an applied compressive strength of 315.88 N for a gradual model; B. deformation with an applied compressive strength of 315.88 N for the gradual model; C. total displacement with an applied compression strength of 315.88 N for the gradual model.

Figure 10 compares the values obtained for the gradual model, using the 2L and 1L tests.

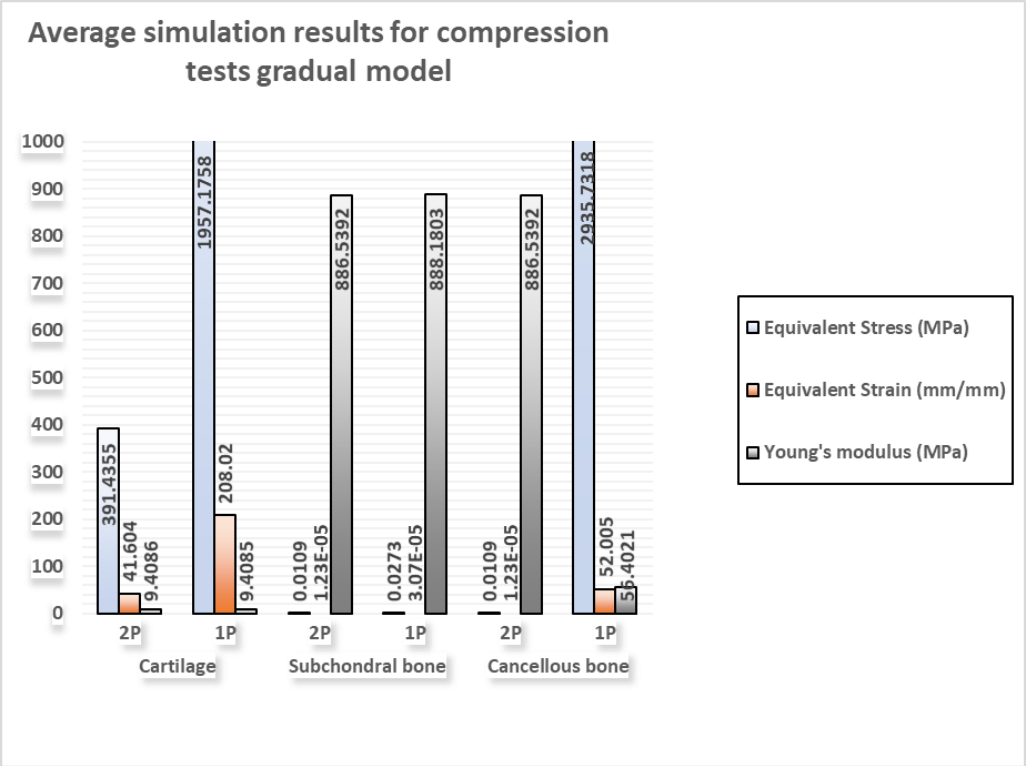

Figure 10 Average simulation results for gradual model compression tests.

3.4 Tensile Tests

3.4.1 Defined Model

The tensile tests were started with a force of 315.88 N, corresponding to position 2L; in the simulation results for the defined model, the highest was 184.61 MPa found in the area for trabecular bone (see Figure 11A), followed by the area for subchondral bone with a maximum of 105.51 MPa, with the cartilage being the smallest value with 79.143 MPa. In contrast to the previous data, cartilage suffered the most significant deformation, with a maximum value of 4.13 mm/mm in light blue in Figure 11B and equal values of 1.3781 mm/mm in the bone areas. The displacement shows a decreasing behavior from the most superficial area of the area for cartilage to the beginning of the area for subchondral bone (Figure 11C).

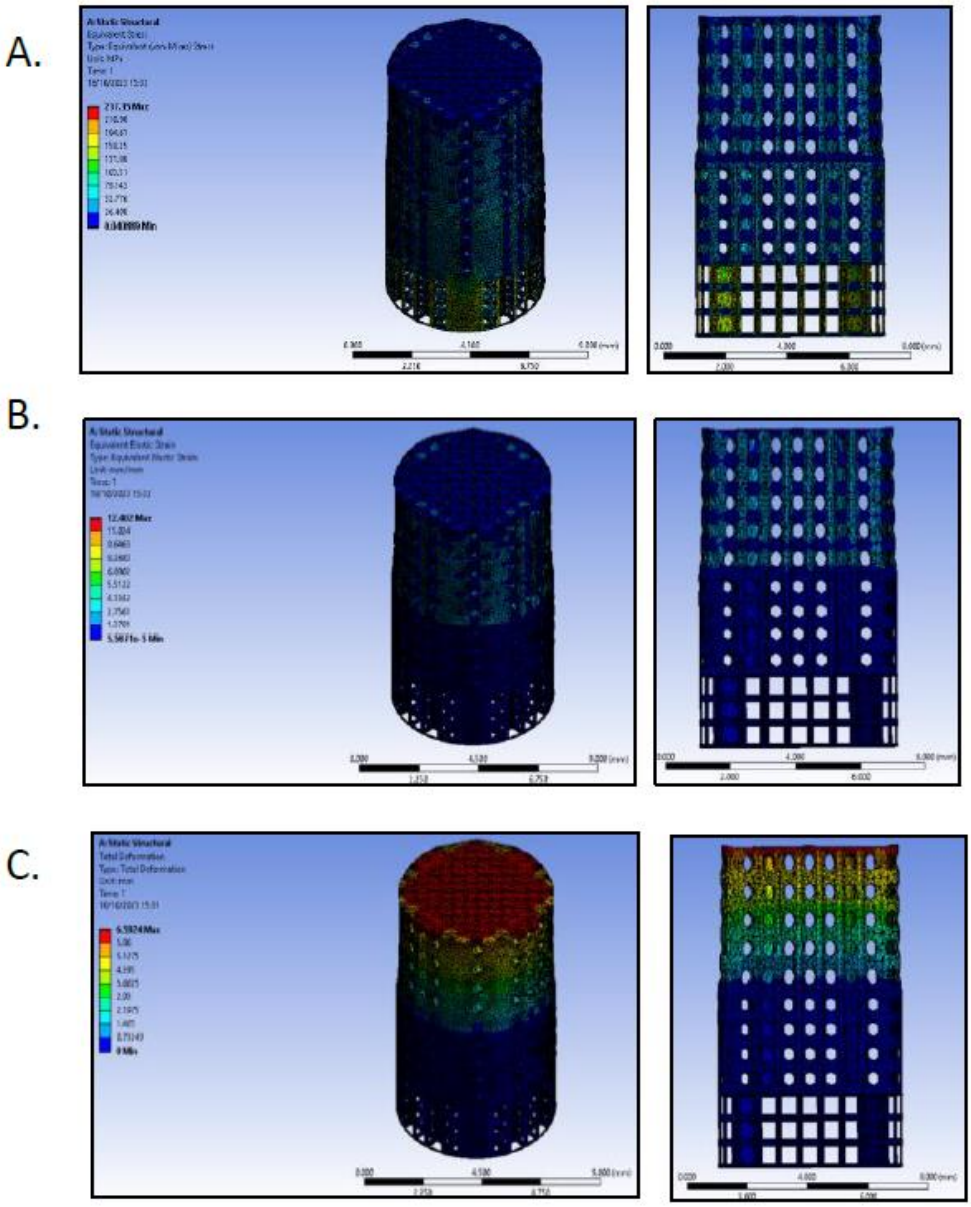

Figure 11 A. Stress distribution with an applied tensile strength of 315.88 N for the defined model; B. deformation with an applied tensile strength of 315.88 N for the defined model; C. total displacement with an applied tensile strength of 315.88 N for the defined model.

There was a difference between the values compared with the 2L and 1L test tests, but the behavior of the scaffold remained the same. Figure 12 shows the comparative graph of the values obtained.

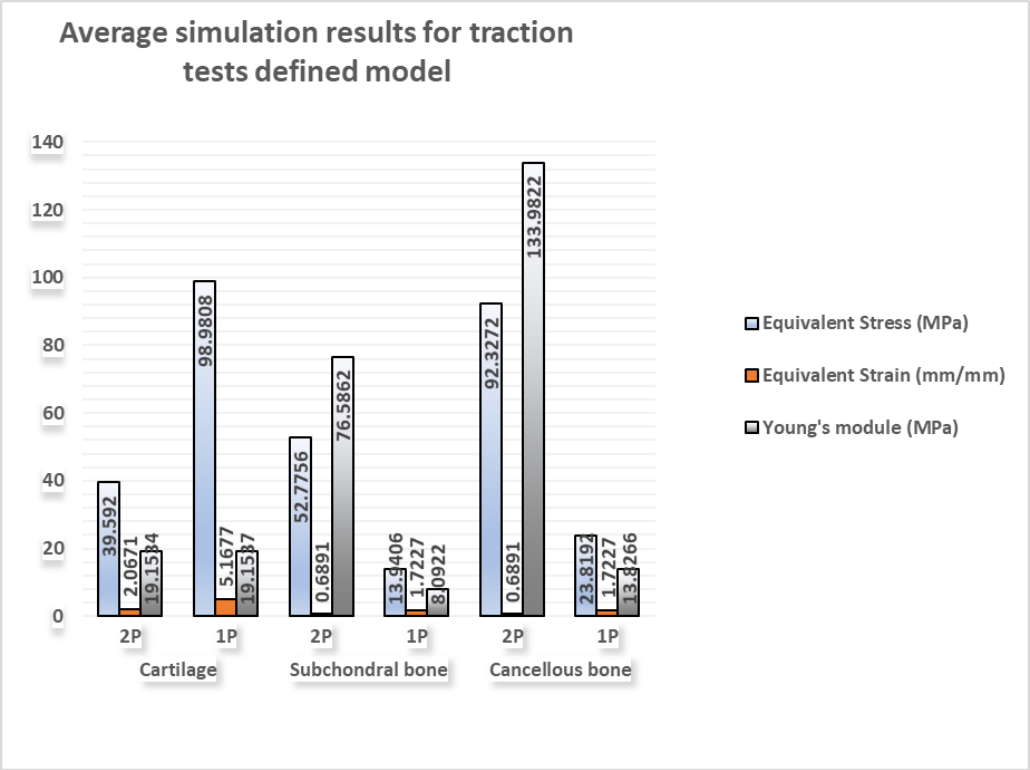

Figure 12 Average simulation results for defined model tensile tests.

In general, the results for the tensile tests were not very constant in all the models, particularly in the defined model; we observed that Young's module for the cartilage area is higher than the real ones for human chondral tissue, even though the values for the two tests remained constant. Regarding the regions for bone, when tested with a force of 789.70 N, the values decreased drastically. However, for the tensile force of 315.88 N, the values were higher; they remained well below the expected parameters.

3.4.2 Truncated Pores Model

In the truncated pores model, the stress distribution we found could have equal results in all the areas in the scaffold with a value of 936.48 MPa, shown in dark blue in Figure 13A. The deformation had the same behavior as in the compression tests but with values ranging from 0.8923 mm/mm to 4.4615 mm/mm and in the bone zones from 0.8923 mm/mm (Figure 13B). The total displacement showed the same behavior as in the previous figures (A and B); see Figure 13C.

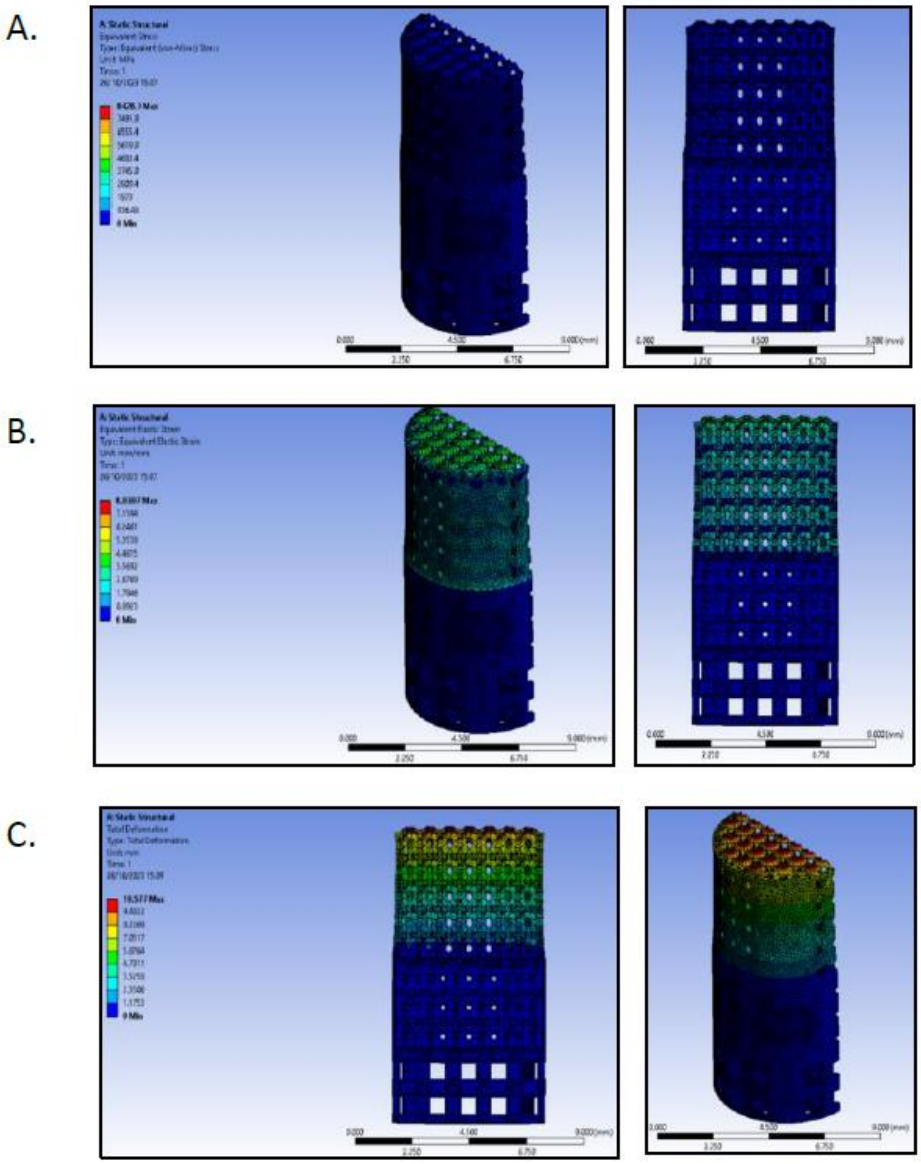

Figure 13 A. Stress distribution with an applied tensile strength of 315.88 N for the truncated pores model; B. deformation with an applied tensile strength of 315.88 N for the truncated pores model and C. Total displacement with an applied tensile strength of 315.88 N for the truncated pores model.

Despite applying more force, the stress distribution for the 1L tests behaved similarly; only the values changed with 2341.7 MPa in both zones for bone (Figure 14).

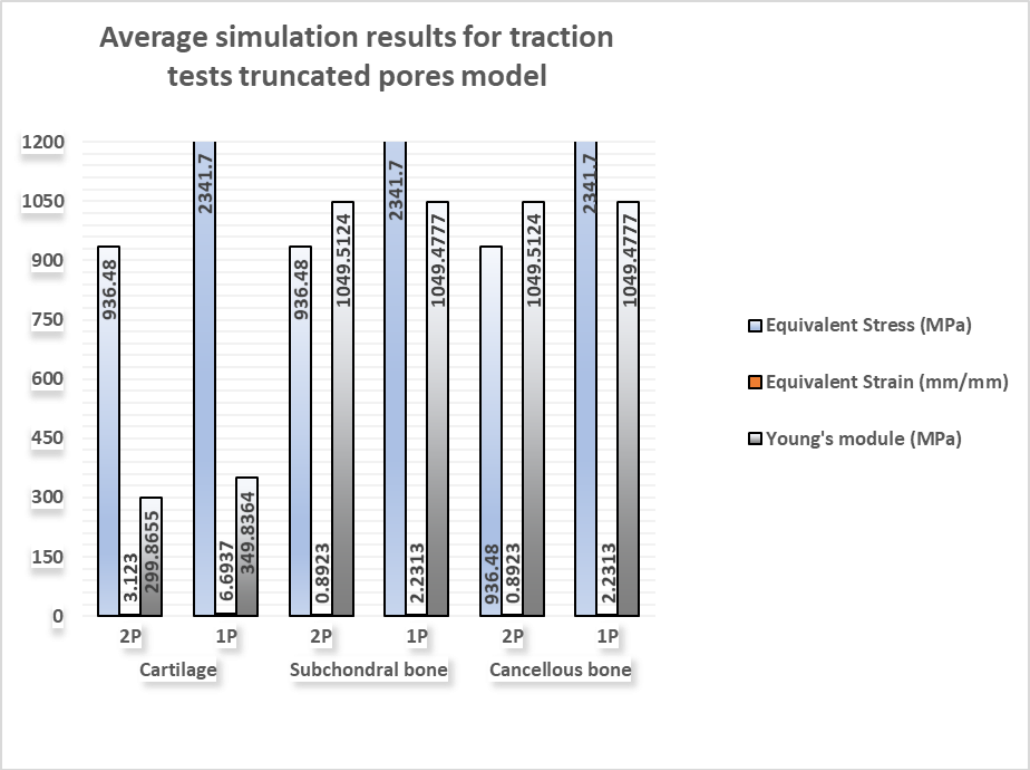

Figure 14 Average simulation results for truncated pore model tensile tests.

As in the compression tests, the values were very constant, almost equal to those in Figure 8. Therefore, the results for the areas of bone were favorable, unlike those for cartilage, which resulted in high values.

3.4.3 Gradual Model

Continuing with the gradual model, the results for the 2L test presented variations in all areas: 1565.7 MPa for cartilage, 782.86 MPa for subchondral bone, and 1565.7 MPa for trabecular bone, as maximum values in light blue (Figure 15A). The tensile strength for equivalent strain had a maximum value of 124.81 MPa for cartilage and 41.604 MPa in both sections for bone (Figure 15B). The total displacement tended to concentrate towards the center of the scaffold (Figure 15C).

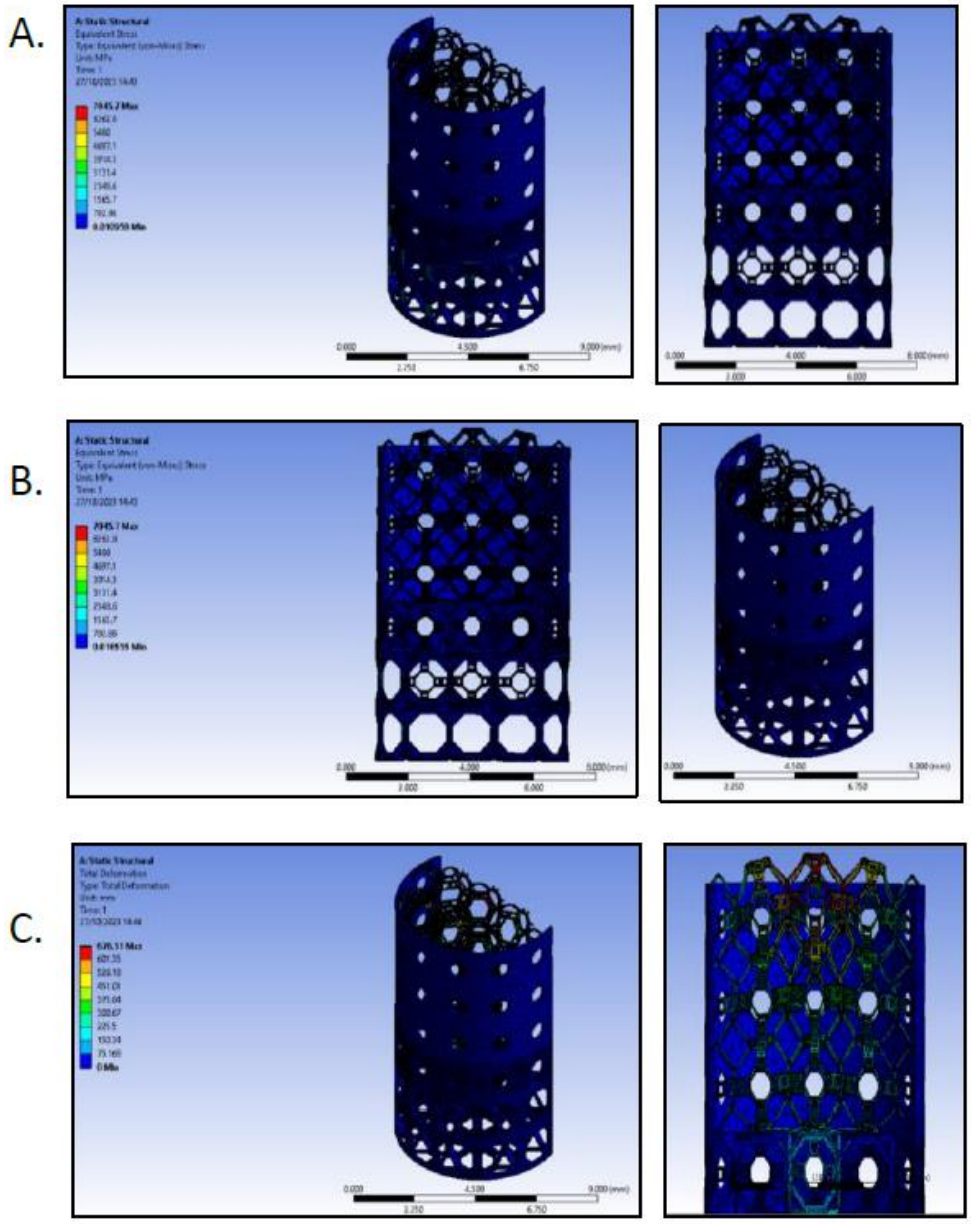

Figure 15 Gradual Model. A. Stress distribution with an applied tensile strength of 315.88 N; B. deformation with an applied tensile strength of 315.88 N and C. Total displacement with an applied tensile strength of 315.88 N.

Figure 16 shows the values for the 2L and 1L tests obtained from the gradual model. Again, the same behavior related to different stresses and deformations in the periphery and the center was detected, as mentioned in the compression tests. Still, the properties changed a little since they were not constant. The values of 6.27 and 14.11 MPa fall within the range of values for Young's modulus of human hyaline cartilage, but what happens is that the higher the force, the higher the modulus increased. This behavior corresponds to the viscoelastic response of cartilage since, in the presence of tensile forces, the behavior is linear, and as the force increases, there is an increase in stiffness [20]. As for the test results for subchondral and trabecular bone, they remained below the expected values; in the former, the values were constant but not in the latter because the stress distribution varied in the periphery of the scaffold.

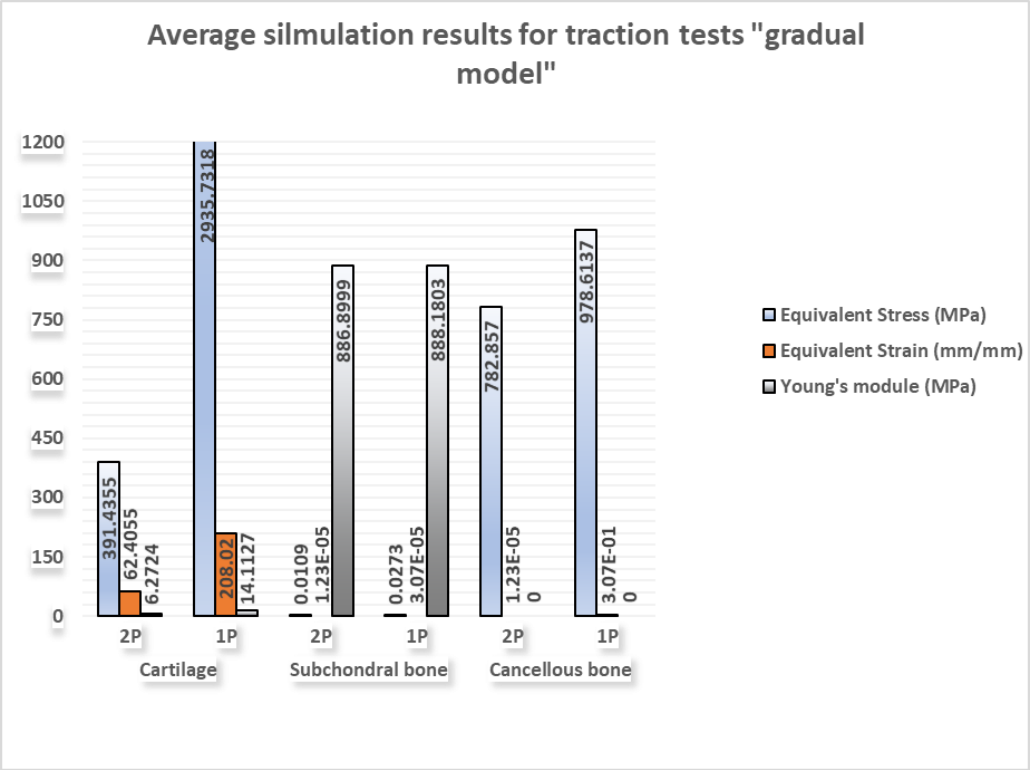

Figure 16 Average simulation results for gradual model tensile tests.

The behavior of the scaffolding was variable, and a comparative analysis was carried out to determine which model had the best results. The values observed in the areas designated for cartilage were significantly higher than expected, as illustrated in Figure 17A, which depicts the minimum and maximum values. The values of Young's modulus for human hyaline cartilage were indicated with dotted horizontal lines. The model with the most significant variation was truncated pores, followed by the defined model. The only model that fell within the acceptable range was the gradual model for both tests. Concerning the subchondral bone area, it was not feasible to ascertain a minimum and maximum value. However, more precise values could be obtained depending on the specific location. The value most closely aligns with this is 1150 MPa, indicated by a horizontal dotted line in Figure 17B. As illustrated in the exact figure, the value exhibiting a degree of variation was 76.67 MPa, obtained in the defined model. In comparison, the truncated and gradual pore models demonstrated a closer alignment with the value observed in human subchondral bone. Continuing with the areas for trabecular bone, the values were very low, the only exception being the truncated pore model. Although the range of values between 1147 and 4590 MPa was more expansive, achieving a more consistent Young's modulus was impossible, as seen in the figures for the two tests (Figure 17C).

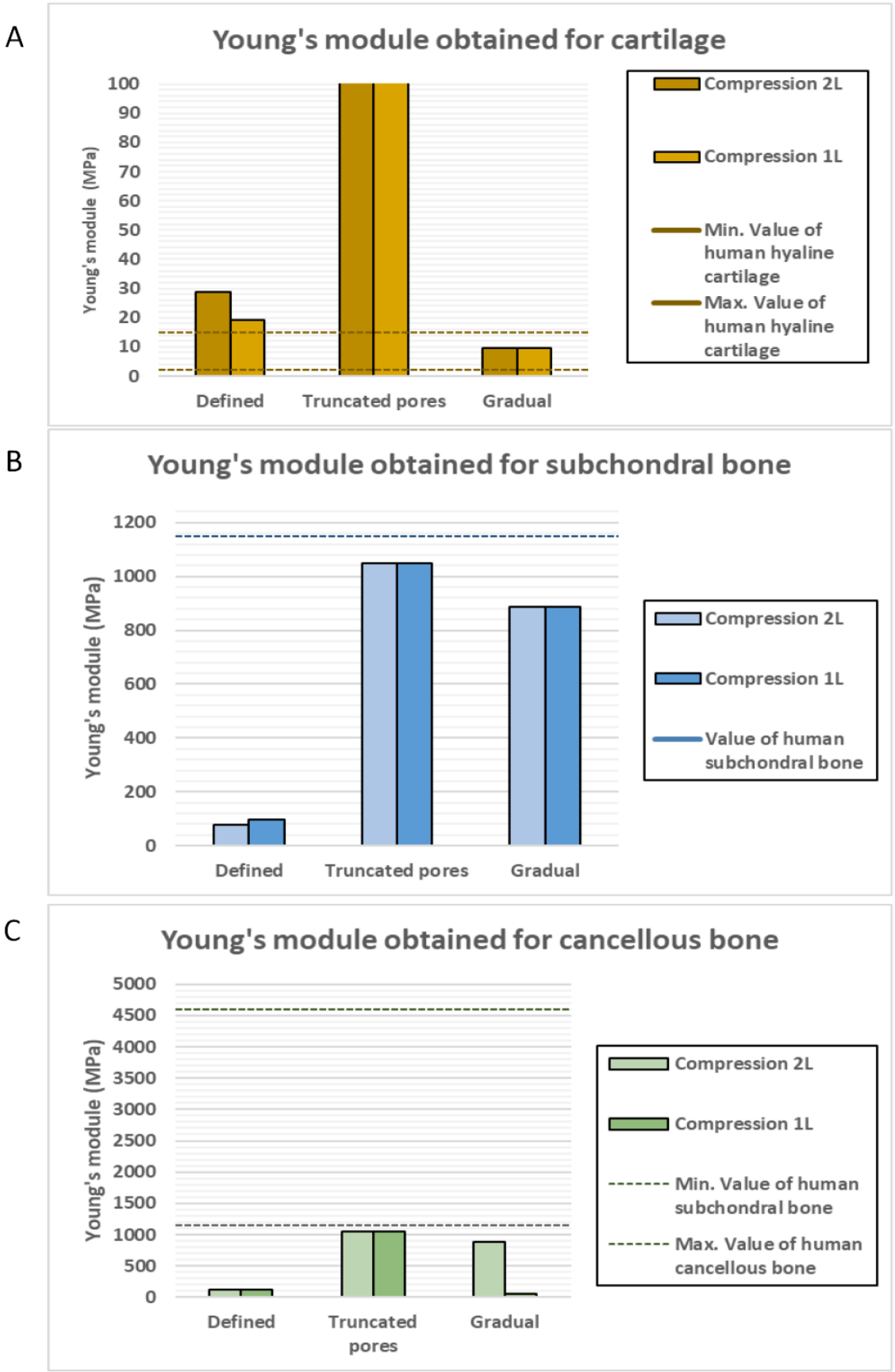

Figure 17 Young's modulus. A. hyaline cartilage. B. subchondral bone. C. trabecular bone.

4. Discussion

We used three distinct unit cells in the “defined” model (see Figure 8). To emulate the characteristics of trabecular bone, we devised tables for the pore geometry, as scaffolds with this configuration facilitate more significant bone growth and are more permeable and stable concerning percentage changes in porosity. This approach enabled us to modify the dimensions of the unit cell more straightforwardly, allowing for the incorporation of two pore sizes within a specified range. A range of pore sizes between 300 and 1000 µm has been demonstrated to facilitate osteogenesis without impeding growth. This encompasses the equivalent pore sizes of 500 and 600 µm, which are 0.5 and 0.6 mm in the case of this scaffold model [8, 21].

Concerning the design of subchondral bone, other research indicates that osteochondral scaffolds typically entail a smooth transition between phases that facilitates the simultaneous regeneration of articular cartilage and subchondral bone. This transition generally has diameters ranging between 170 and 195 µm, as evidenced by references [16, 21]. Consequently, a primary pore size of 200 µm (or 0.2 mm in the design) was selected for this tissue, while a secondary pore size of 350 µm was also considered. Geometrically, the pore design was chosen to be a hexagonal configuration. Ramin Rahmani and colleagues had previously concluded that their five-design approach, precisely the honeycomb configuration, exhibited superior cell growth outcomes [22].

It is crucial to highlight that tiny pores with a diameter range of 100 to 120 µm facilitate hypoxic conditions with low oxygen tension, constraining vascular invasion and promoting chondrogenesis [12]. However, these small diameters are often undetectable or barely perceptible during the fabrication of a tangible model. Therefore, based on an investigation that successfully achieved chondrocyte proliferation using scaffolds with smooth fibers of 250 µm in diameter [19], this same diameter was selected as the most critical pore in the design of the area for hyaline cartilage, applied to the horizontal diameter of the pores in the ellipse. Similarly, the secondary pore size for the cartilage area was 350 µm, but with an octagonal shape. This geometry was selected based on the findings of simulations conducted by S. Karuppudaiyan and colleagues, which indicated that it resulted in a lower Young's modulus, a desirable property for this type of tissue given its biomechanical characteristics [23].

The geometry and pore size are of significant importance in the design of scaffolds. Consequently, the truncated pore model employed varying sizes of unit cells and a geometry for unit cells of hollow hexahedra with cuts in all vertices and perforations in each face. The results obtained by S. Karuppudaiyan and colleagues indicate that a unit cell with a truncated hexahedron geometry exhibits a high Young's modulus, although not as high as a complete hexahedron [24]. This is a crucial consideration when mimicking bone and cartilage, as Young's module of these tissues exhibits a range of magnitudes. Another pertinent study indicated that bone development and growth cells might exhibit a proclivity for larger pore sizes. In the design of their scaffold, they utilized circular rods of approximately 1.3 mm in diameter, positioned one atop the other with a 1 mm interval [25]. Accordingly, the largest unit cell, which corresponds to the osseointegrate zone for trabecular bone, was designed with dimensions of 1.2 mm × 1.2 mm × 1.2 mm, extending until reaching the zone for cartilage with dimensions of 0.8 mm × 0.8 mm × 0.8 mm (see Figure 2).

The initial model established that Young's modulus values of cartilage and bone are markedly disparate, with the former exhibiting a significantly lower range, between 2 and 15 MPa, compared to the latter, which ranges from 300 MPa for trabecular bone to 15 GPa for compact bone, as

documented in the literature [26]. The values obtained for Young's modulus exhibited considerable discrepancies from the actual values of osteochondral tissue. However, when compared with a predictive study of optimal mechanical properties for osteochondral defect repair, the authors proposed reducing the modulus of a scaffold from 60 MPa to 10 MPa from the superficial layer to the base of the chondral zone [27]. As shown in Figure 5C, the area with the most significant displacement is the cartilage region, where higher values are found in the superficial layer and decrease uniformly until reaching the subchondral bone area. This evidence backs the assertion that a cushioning function is provided, aiding in the transfer of loads. Movement within the cartilage area encourages and stimulates cartilage metabolism.

In contrast, the truncated pore model shows a more constant but less favorable behavior for the values sought since 2L and 1L were almost identical in all areas. In the area of cartilage, Young's modulus remains at the same value in the two tests but with high values. On the other hand, for the subchondral bone area, the results were satisfactory since, according to an article about the biomechanics of the osteochondral tissue, Young's modulus value is 1150 MPa, almost equal to the one obtained in this scaffold [8, 28]. On the other hand, the standard value of Young's modulus for trabecular bone, also mentioned in this article, is between 1147 MPa and 4590 MPa, which is in an acceptable range, and the total displacement is evenly distributed across the cartilage area. It decreases to a minimum value just before reaching the trabecular bone zone, adhering to the characteristic damping property of cartilage. This behavior was similar in the tensile tests, except that higher values were recorded in the cartilage area.

The gradual model exhibited unanticipated behavior, as evidenced by the disparate stresses and deformations observed in the cartilage area. The sheet operation, which encompasses the contour of the model and its interior, demonstrated varying stress levels. The applied stresses were notably higher in the model's center, while the periphery exhibited a constant value similar to the remaining areas. Notwithstanding the observations above, the average value for Young's modulus for this area yielded satisfactory and consistent results for the 2L and 1L tests. According to the literature, the implantation of a non-homogeneous scaffold, where Young's modulus is reduced from 60 to 10 MPa, facilitates the formation of osteochondral tissue. This tissue is characterized by a distinct composition, with chondral tissue in the cartilage region and bone tissue in the area of bone [27]. Notwithstanding the favorable outcomes in the anterior region, the subchondral and trabecular bone results remained below the anticipated values. In the former, the values exhibited constancy, whereas in the latter, the stress distribution exhibited variability at the periphery of the scaffold. The displacement tended to converge towards the center, encompassing approximately two-thirds of the model. This was not an optimal outcome, as it did not yield a uniform and favorable distribution to fulfill a damping function.

5. Conclusions

Three scaffold models featuring various geometric shapes and specific pore sizes were developed and assessed for design and simulation using SolidWorks and Ansys Workbench to investigate the mechanical properties of bone and cartilage. The load simulations, both compression and traction, showed that the truncated and gradual pore models better fit the subchondral bone and hyaline cartilage parameters. Scaffolds can withstand physiological loads without failing, with deformations concentrated in the cartilage areas and a gradual decrease in the bone areas.

Comparative mechanical analysis shows inconsistent results, showing variability in each model. In the truncated pore model, the values for cartilage were significantly elevated compared to those observed in human cartilage. The subchondral bone showed an inverse response in the defined model, with values lower than expected. In addition, the graded model showed values for the trabecular bone area below the expected range. When designing these scaffolds, it is advisable to create a thicker structure in the trabecular bone area or a thinner structure in the cartilage and subchondral bone areas [28, 29].

In conclusion, scaffold designs must have a previous structural analysis to see the effects of the mechanical loads before their manufacture and application [8]. This study has provided valuable insights into the design of hybrid scaffolds with lattice structures for osteochondral regeneration. The results suggest that combining scaffold architectures, especially the truncated and gradual pore models, could effectively regenerate articular cartilage and underlying bone. Future research could explore the optimization of these designs and their application *in vitro* trials to validate their effectiveness in repairing grade IV chondral lesions and their use in 3D printing models.

6. Future Perspectives

Carry out new simulations of the models with different biomaterials, especially biopolymers, to study their mechanical behavior with the proposed structures and those presented by other authors [11-13].

The wall thickness for trabecular tissue models should be increased or reduced for subchondral tissue and cartilage zones to improve the biomechanics of the proposed models.

Replicate models with different pore sizes and observe if the mechanics of the structures vary with the loads previously established in this work.

Carrying out stress tests considering the forces exerted by tendons on joints would give us a better understanding of the models' behavior and their interaction with other types of tissue.

Acknowledgments

The authors would like to thank CONAHCYT for the economic stimulus provided through the National System of Researchers.

Author Contributions

J Palacios: Methodology, Software, formal analysis, writing – original draft. O Ramírez-Fernández: Software, formal analysis. E Zuñiga-Aguilar: Conceptualization, writing – original draft, writing – review and editing. All authors have read and approved the published version of the manuscript.

Competing Interests

The authors have declared that no competing interests exist.

References

1. Moarrefzadeh A, Morovvati MR, Angili SN, Smaisim GF, Khandan A, Toghraie D. Fabrication and finite element simulation of 3D printed poly L-lactic acid scaffolds coated with alginate/carbon nanotubes for bone engineering applications. Int J Biol Macromol. 2023; 224: 1496-1508.
2. Forriol Campos F. Articular cartilage: Mechanical factors and their effects on tissue repair. Rev Ortop Traumatol. 2002; 46: 380-390.
3. Álvarez E, Ripoll PL, Restrepo A, Forriol F. Revisión de la reparación del cartílago. Posibilidades y resultados. Trauma. 2010; 21: 117-134.
4. Gallegos Nieto E, Medellín Castillo HI, De Lange DF. Análisis del desempeño estructural de andamios de hidroxiapatita utilizados en ingeniería tisular. Ing Mecánica Tecnol Desarrollo. 2013; 4: 185-194.
5. Egan PF, Gonella VC, Engensperger M, Ferguson SJ, Shea K. Computationally designed lattices with tuned properties for tissue engineering using 3D printing. PloS One. 2017; 12: e0182902.
6. Tang Y, Dong G, Zhao YF. A hybrid geometric modeling method for lattice structures fabricated by additive manufacturing. Int J Adv Manuf Technol. 2019; 102: 4011-4030.
7. Egan PF, Shea KA, Ferguson SJ. Simulated tissue growth for 3D printed scaffolds. Biomech Model Mechanobiol. 2018; 17: 1481-1495.
8. Zuñiga-Aguilar E, Ramírez-Fernádez O, Botello-Arredondo A. Desing and simulation of scaffolds with lattice microstructures for bioprinting bone tissue. Bio-Med Mater Eng. 2024; 35: 415-423.
9. Nogueira P, Castresana K, Magrinho J, Silva MB, de Deus AM, Vaz MF. Computational evaluation of the compressive properties of different lattice geometries to be used as temporary implants. Procedia Comput Sci. 2023; 217: 928-937.
10. Sun W, Starly B, Nam J, Darling A. Bio-CAD modeling and its applications in computer-aided tissue engineering. Comput Aided Des. 2005; 37: 1097-1114.
11. Karimi M, Asefnejad A, Aflaki D, Surendar A, Baharifar H, Saber-Samandari S, et al. Fabrication of shapeless scaffolds reinforced with baghdadite-magnetite nanoparticles using a 3D printer and freeze-drying technique. J Mater Res Technol. 2021; 14: 3070-3079.
12. Li X, Saeed SS, Beni MH, Morovvati MR, Angili SN, Toghraie D, et al. Experimental measurement and simulation of mechanical strength and biological behavior of porous bony scaffold coated with alginate-hydroxyapatite for femoral applications. Compos Sci Technol. 2021; 214: 108973.
13. Iranmanesh P, Gowdini M, Khademi A, Dehghani M, Latifi M, Alsaadi N, et al. Bioprinting of three-dimensional scaffold based on alginate-gelatin as soft and hard tissue regeneration. J Mater Res Technol. 2021; 14: 2853-2864.
14. Amador-Rosales PY. Diseño de patrones de impresión tipo gyroid lattice para un andamio enfocado a la bioimpresión de tejido cartilaginoso hialino. Ciudad Juárez, Mexico: Universidad Autonoma de Ciudad Juarez; 2020.
15. Kutzner I, Heinlein B, Graichen F, Bender A, Rohlmann A, Halder A, et al. Loading of the knee joint during activities of daily living measured in vivo in five subjects. J Biomech. 2010; 43: 2164-2173.
16. Li JJ, Kim K, Roohani-Esfahani SI, Guo J, Kaplan DL, Zreiqat H. A biphasic scaffold based on silk and bioactive ceramic with stratified properties for osteochondral tissue regeneration. J Mater Chem B. 2015; 3: 5361-5376.

17. Harley BA, Lynn AK, Wissner-Gross Z, Bonfield W, Yannas IV, Gibson LJ. Design of a multiphase osteochondral scaffold III: Fabrication of layered scaffolds with continuous interfaces. J Biomed Mater Res A. 2010; 92: 1078-1093.
18. Ali D, Sen S. Finite element analysis of mechanical behavior, permeability and fluid induced wall shear stress of high porosity scaffolds with gyroid and lattice-based architectures. J Mech Behav Biomed Mater. 2017; 75: 262-270.
19. Horas U. Defectos condrales de la rodilla tratados mediante autotrasplante de cilindros osteocondrales. Tec Quir Ortop Traumatol. 2023; 12: 48-62.
20. Rodríguez-Camacho DF, Correa-Mesa JF. Biomecánica del cartílago articular y sus respuestas ante la aplicación de las fuerzas. Medicas UIS. 2018; 31: 47-56.
21. Karageorgiou V, Kaplan D. Porosity of 3D biomaterial scaffolds and osteogenesis. Biomaterials. 2005; 26: 5474-5491.
22. Rahmani R, Antonov M, Kollo L, Holovenko Y, Prashanth KG. Mechanical behavior of Ti6Al4V scaffolds filled with $CaSiO_3$ for implant applications. Appl Sci. 2019; 9: 3844.
23. Woodfield TB, Malda J, De Wijn J, Peters F, Riesle J, van Blitterswijk CA. Design of porous scaffolds for cartilage tissue engineering using a three-dimensional fiber-deposition technique. Biomaterials. 2004; 25: 4149-4161.
24. Karuppudaiyan S, Singh DK, Santosh VM. Finite element analysis of scaffold for large defect in femur bone. IOP Conf Ser Mater Sci Eng. 2018; 402: 012096.
25. Jiang CP, Chen YY, Hsieh MF. Biofabrication and in vitro study of hydroxyapatite/mPEG–PCL–mPEG scaffolds for bone tissue engineering using air pressure-aided deposition technology. Mater Sci Eng C. 2013; 33: 680-690.
26. Armstrong CG, Mow VC. The mechanical properties of articular cartilage. Bull Hosp Jt Dis Orthop Inst. 1983; 43: 109-117.
27. Kelly DJ, Prendergast PJ. Prediction of the optimal mechanical properties for a scaffold used in osteochondral defect repair. Tissue Eng. 2006; 12: 2509-2519.
28. McMahon LA, O 'Brien FJ, Prendergast PJ. Biomechanics and mechanobiology in osteochondral tissues. Regen Med. 2008; 3: 743-759.
29. Yu L, Cavelier S, Hannon B, Wei M. Recent development in multizonal scaffolds for osteochondral regeneration. Bioact Mater. 2023; 25: 122-159.